ASME Journal of Computational and Nonlinear Dynamics
Online journal at:
https://asmedigitalcollection.asme.org/computationalnonlinear

A Comprehensive Method for Computing Non-Linear Elastokinematic Properties of Passenger Car Suspension Systems: Double Wishbone Case Study

Paolo Magri[1]
Department of Mechanical and Industrial Engineering, University of Brescia, Brescia I-25123, Italy
e-mail: p.magri003@unibs.it

Marco Gadola
Department of Mechanical and Industrial Engineering, University of Brescia, Brescia I-25123, Italy

Daniel Chindamo
Department of Mechanical and Industrial Engineering, University of Brescia, Brescia I-25123, Italy

Giulia Sandrini
Department of Mechanical and Industrial Engineering, University of Brescia, Brescia I-25123, Italy

Suspension and steering design play a major role in ensuring the correct dynamic behavior of road vehicles. Passenger cars are especially demanding from this point of view: NVH and ride comfort requirements often collide with active safety-related requirements such as road holding in steady-state conditions and stability in transients. Driving pleasure is also important for market success, therefore accurate steering feedback and predictable handling properties are additional priorities. Since flexible bushings are used as interface between the suspension arms and the chassis, extra degrees-of-freedom make the design process a complex task. While the use of a multibody software is common practice in the industry, a dedicated computational tool can be more practical and straightforward, especially when undertaking the design of a new suspension concept ground-up. The paper presents a computational methodology for the design of an independent suspension with the associated kinematic and compliance attributes. Typical elastokinematic properties like toe, camber, wheelbase, and track variations versus tyre forces and moments can be computed by means of a dedicated software tool. A sort of validation was performed either by means of a comparison with a MathWorks Simscape® Multibody based model. Finally, a sensitivity analysis is given as an example. Computationally, the method proposed is intuitively based on the equilibrium equations. The nonlinear equations are then solved with Newton–Raphson algorithm. The method can be also optimized for computational efficiency and is thoroughly described so that the reader can easily replicate it in the desired programing environment. [DOI: 10.1115/1.4066092]

Keywords: computational kinematics and dynamics, computational mechanics, nonlinear phenomena, vehicular dynamics, vehicle suspension, elasto-kinematics

1 Introduction

Modern passenger cars require an intensive effort for the design of suspension elastokinematic properties because of their relevant impact on ride and handling. This is reflected in a vast engineering literature on the subject. The use of multibody models, for instance, although being the industry standard, is often considered demanding because of the high level of details required. The development and application of relatively simple, dedicated design and simulation tools instead is often considered more practical, especially when designing a new suspension concept ground up. This tendency is clearly visible in the related literature as many publications describe self-developed, peculiar methodologies, often responding to a varied level of complexity as well as to a different computational approach. A multibody model is often used as validation in these cases.

The so-called multilink rear suspension concept was introduced in the early eighties by Mercedes with the W201 (190) model, which represented a leap forward in terms of elastokinematics. The design requirements aimed at decoupling longitudinal compliance and wheel guidance, as well as the innovative way they were achieved are accurately described in Ref. [1], which is considered a milestone in the related literature. FEM analysis on suspension link deflection was used in order to simulate the deflection of rubber bushings.

Among other efforts, significant contributions on design requirements for suspension kinematics and elastokinematics have been released by Volvo [2], Nissan [3,4], Hyundai-Kia [5], and Ford [6], with the latter focused on the so-called integral link geometry. Analyzing the literature in the automotive field, pure kinematics is dealt by Gerrard in Ref. [7]. Another effort from the same author regarding kinematics synthesis is given in Ref. [8], where significant limitations also occur, small displacements around the design

[1]Corresponding author.

Manuscript received September 29, 2023; final manuscript received July 4, 2024; published online August 22, 2024. Assoc. Editor: Andreas Mueller.

configuration apply, and the interposition of elements between suspension linkages is not considered, that is to say a layout like the integral link cannot be modeled. Kinematics is also on focus in Ref. [9], while the synthesis of five-link kinematics is discussed in Refs. [10] and [11]. This is a relevant subject, even when neglecting elastokinematics, due to the optimization complexity with so many design variables available to play with.

Pure kinematics computation is also used for applications related to motorsport [12–14] and for educational purposes as well [15]. The integration of a dedicated software with a toolchain for vehicle dynamics simulation is presented in Ref. [16]. It features a built-in graphical user interface conceived to facilitate the kinematics design process.

Papers from well-known authors Knapczyk et al. are cited quite often. Among many, Ref. [17] still refers to Ref. [1] as a case study and reports a method for computing the force/displacement relationship of a five-rod multilink suspension based on the vector algebraic method. Rubber bushings are described in detail, although their stiffness is considered in the radial and axial directions only. While Ref. [18] mainly deals with vertical dynamics, an approach similar to Ref. [17] is found in Ref. [19], where the role of the subframe (also referred to as "bogie" in its typical arrangement, i.e., connected to the chassis by four, vertical-axis, large rubber bushings) is also taken into account in order to simulate the elastokinematic behavior of the rear axle as a whole. Again, from the same authors comes [20], dealing once again with a rear, five-link suspension, although with attention to vertical dynamics as well.

The contribution of rubber bushings is considered in Ref. [21], where a comprehensive model of a double-wishbone front suspension is used for durability simulations, with specific focus on the angular travel of ball joints fitted at the outer end of both the lower and upper control arms as well as at both ends of the steering rod. Bushings feature nonlinear characteristics in the axial, radial, torsional, and conical directions.

Various authors adopted the equivalent stiffness approach in order to correlate suspension geometry and rubber bushing characteristics to the stiffness at the wheel center. This method is strongly focused on the design of kinematics and compliance properties of the suspension as a whole. Compliance properties are computed at the wheel center as a function of linear bushing characteristics in Ref. [22]. Kinematics is neglected in this case, as it is in Ref. [23]. In this case the same authors take link flexibility into account as well.

Another interesting effort based on the stiffness matrix is Ref. [24], from the same author of Refs. [7] and [8]. Once again, however, the paper deals with small displacements and linear bushings, which should be seen as an important limitation given their typically nonlinear behavior [21].

Elastokinematics is the subject of papers focusing on the MacPherson layout as well. Examples are given in Refs. [25] and [26], where the bushing stiffness is considered in the radial and axial directions and fully linear.

An extensive sensitivity analysis is carried out in Ref. [27], focusing on the interactions between steering kinematics, antiroll bar rate, elastokinematics, and handling response of a front-wheel-drive passenger car by means of multibody modeling. The correlation between elastokinematic modeling and experimental testing on Michelin's well-known K&C (kinematics & compliance) test rig is the subject of Ref. [28]. Rubber bushings are modeled quite accurately, while according to the authors ball joint friction and the visco-elastic properties of rubber also play an important role in the overall suspension behavior.

Starting again from experimental data, reverse engineering of the three translational bushing characteristics is the aim of Ref. [29]. In this case, rubber joints can be placed either side of each suspension link. All bushing characteristics however are de-emed as linear: this is a typical case study of an identification process. It also seems that the assumption of variable length suspension links might require further assessment. Nonlinear stiffness of bushings along all six degrees-of-freedom is instead adopted in Ref. [30], aimed at the computation of joint forces on the chassis side of a double-wishbone suspension. In this work, which in the author's opinion seems to be one of the most complete, the wheel-side bushings are not considered, and all elements except the spring are rigid. However, the spring is considered as a simple elastic element without considering that it is often mounted on the frame and suspension by means of rubber bushings. The nonlinearity of stiffnesses is considered by means of force–displacement curves composed of several linear segments.

Finally, the methodology behind an earlier version of the well-known commercial tool Shark® by Lotus Engineering is described in Ref. [31]. In this tool, both wheel-side and frame-side bushings can be inserted, but limitations remain: stiffnesses can only be linear. Also, the kinematics of the system is not taken into account; the tool calculates the stiffness matrix of the suspension, linearizing it, but this is only good for small deformations.

As a general rule, most of the papers in the literature tend to neglect one or more factors of the real-world design. Either the bushings are represented with linear characteristics or with nonlinear curves but only for translational displacements, i.e., in the axial and radial directions only, while the angular deflection rates are not considered. Another limitation that is often found is the fact that rubber bushings are featured on the chassis side of suspension arms only, while in current suspension systems they are sometimes located between the suspension arms and the wheel carrier as well, or even in the middle of the trackrod. Some papers also tend to linearize suspension behavior in a small displacement range around the static or design configuration with a single stiffness matrix.

This paper proposes an algorithm that can overcome all the above-mentioned related problems, attempting to create a comprehensive methodology. Above all, this paper can be able to fully handle the nonlinear stiffness characteristics typical of bushings. Purpose of this work is to provide a method for the solution of the suspension elastokinematic problem, by means of a general method enabling the design of most of the modern layouts, from simple semitrailing arms to all kinds of suspensions with a virtual instantaneous axis of rotation in steering or under load, including the so-called integral link geometry. Bushings can be described with their stiffness properties for all six degrees-of-freedom and with real-world, nonlinear curves. They can be located either side of each suspension arm, i.e., on the chassis side and/or on the wheel side. The flexibility of trackrod can also be represented by means of equivalent, nonlinear bushings. The wheel bearing stiffness can be considered as well. Wheel movement hence variations of vehicle dynamics-relevant parameters like camber, side view angle, toe, track, wheelbase and vertical displacement can be computed under any combination of road loads: braking, traction, cornering and bump impacts. Any combination of jounce and steer motion can be simulated within the whole range allowed by bump and rebound stop. Suspension's joints and chassis loads can also be computed.

The proposed algorithm has been presented in a general mathematical formulation; however, it has been implemented in the Matlab environment. This environment was chosen as it specializes in matrix calculation and allows the programmer to write vectors, matrices, and operations between them in an intuitive way, and is characterized by good computational speed despite being a high-level language. The Matlab environment also allows interfacing with Simulink, enabling the user to implement other functions, e.g., implementing optimization logic or sensitivity analysis. However, Matlab is not freely accessible, and this may be the main limitation. An excellent alternative could be Python, using existing mathematical libraries. Another alternative, which would guarantee higher computation speeds than Matlab, could be to implement the code in C++, although this is less intuitive to code.

2 Suspension Model Description

In this model, two types of elements are considered. The first type of element is called "spring rod" and it is composed by two bushings at the ends and a rod with an axial stiffness. The second element is

called "rigid element" and it is composed by a rigid body with any number of bushings. The two elements are shown in the Fig. 1.

Any element can be attached to each other element or to the ground. The elements connected to each other share a bushing. Otherwise, the element is attached to the ground by linking its bushing to the global reference system (GRS) which represents the body chassis of the vehicle.

By combining these elements, it is possible to create any type of independent suspension. For example, in a double wishbone, the two wishbones will consist of a rigid element connected to the chassis by two bushings and to the upright by one bushing. The upright will also be a rigid element with three bushings, two connected to the wishbones and one to the steering tie rod; this one will instead be modeled using a spring rod element. A Multilink suspension can be easily modeled using five spring rods for the arms and a rigid element with five bushings for the hub carrier. A MacPherson strut can also be modeled by constraining a spring rod between the chassis and the hub carrier and making the bushing that connects them infinitely rigid. It is also possible to create an integral link suspension attaching a spring rod between the wishbone and the upright.

Finally, to calculate the elastokinematics configuration under lateral load more realistically, it is possible to steer the suspension by moving the attachment point on the chassis side of the steering rod.

2.1 Bushings Definition. By playing with bushing stiffnesses, it is also possible to exclude the elastic component. For example, by increasing the translation stiffness by a few orders of magnitude and decreasing the rotation stiffness, it is possible to turn the bushing into ball joints. Figure 2 represents the bushing model described in this work.

Each bushing must be defined with its position $Xb = [xb\ yb\ zb]$ in the GRS and with three angles $\theta b = [\theta b_x\ \theta b_y\ \theta b_z]$, with which it is therefore possible to define a rotation matrix $[R]$ to identify the orientation of the bushing in the GRS. The bushing is defined by a function "*Reaction Forces Vector*" (1) that contains six functions that correspond to the three reaction forces and the three reaction moments generated by the bushing as a function of the six deformations ub^{LRS} of the bushing itself

$$Fb(b^{\mathrm{LRS}})^{\mathrm{LRS}} = \begin{bmatrix} Fb_x(ub_x) \\ Fb_y(ub_y) \\ Fb_z(ub_z) \\ Fb_{rx}(ub_{rx}) \\ Fb_{ry}(ub_{ry}) \\ Fb_{rz}(ub_{rz}) \end{bmatrix} \tag{1}$$

where "LRS" stays for local reference system. Both the deformations and the reaction forces vector are defined in the LRS in this case. Knowing the rotation matrix $Rb(\theta b)$ that identifies the orientation of the bushing, it is possible to calculate the reaction force in the GRS (2).

$$Fb(ub)^{\mathrm{GRS}} = [Rb_{\mathrm{exp}}] \cdot Fb\Big([Rb_{\mathrm{exp}}]^T \cdot (ub^{\mathrm{GRS}})\Big)^{\mathrm{LRS}} \tag{2}$$

where $[Rb_{\mathrm{exp}}]$ is the *expanded* rotation matrix (3) that is defined as follows:

$$[Rb_{\mathrm{exp}}(\theta b)] = \begin{bmatrix} [Rb(\theta b)] & 0 \\ 0 & [Rb(\theta b)] \end{bmatrix} \tag{3}$$

The rotation matric Rb is calculated with a Tait-Bryan transformation (4) $X_1Z_2Y_3$.

$$Rb(\theta b) = [\mathrm{rot}x(\theta b_x)] \cdot [\mathrm{rot}z(\theta b_z)] \cdot [\mathrm{rot}y(\theta b_y)] \tag{4}$$

where

$$[\mathrm{rot}x(\alpha)] = \begin{bmatrix} 1 & 0 & 0 \\ 0 & \cos\alpha & -\sin\alpha \\ 0 & \sin\alpha & \cos\alpha \end{bmatrix} \tag{5}$$

$$[\mathrm{rot}y(\alpha)] = \begin{bmatrix} \cos\alpha & -\sin\alpha & 0 \\ \sin\alpha & \cos\alpha & 0 \\ 0 & 0 & 1 \end{bmatrix} \tag{6}$$

$$[\mathrm{rot}z(\alpha)] = \begin{bmatrix} \cos\alpha & 0 & \sin\alpha \\ 0 & 1 & 0 \\ -\sin\alpha & 0 & \cos\alpha \end{bmatrix} \tag{7}$$

Each function of Fb can be any function of the deformation ub, even nonlinear.

2.2 Element Definition. For the spring rod element, a function $Fa(ua)$ is also defined that represents the axial elastic force as a function of the axial deformation of the element. It can also be any function, just like for the bushings. The force–displacement curve that characterizes the spring element can be generated at will. It is also possible to insert a preload value as a displacement. Each i-th element of the suspension is described by a vector $u_i^{\mathrm{GRS}} = [u_x\ u_y\ u_z\ u_{rx}\ u_{ry}\ u_{rz}]$ containing the displacement of one of its bushings from its design position and by its axial displacement ua_i if it is a *spring rod* element. The displacement vector of the other bushings of the element can be easily calculate trough transformation matrix because the element is a rigid body. To calculate the deformed configuration of the suspension is necessary to know all the deformation vector and axial deformation of each element. The vector (8) containing these vectors is defined as follows:

$$U = [u_1^{\mathrm{GRS}}\ u_2^{\mathrm{GRS}}\ \ldots\ u_n^{\mathrm{GRS}}\ ua_1\ ua_2 \ldots ua_n] \tag{8}$$

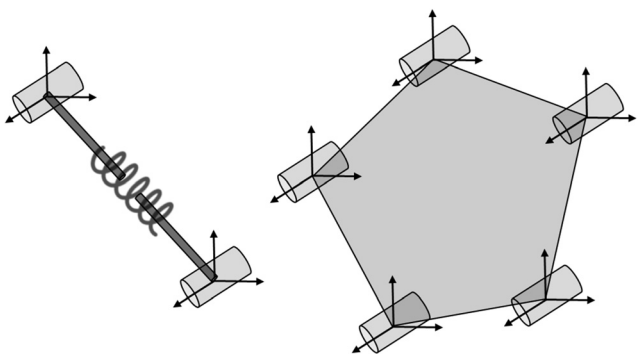

Fig. 1 General "spring rod" and "rigid element" of the suspension model

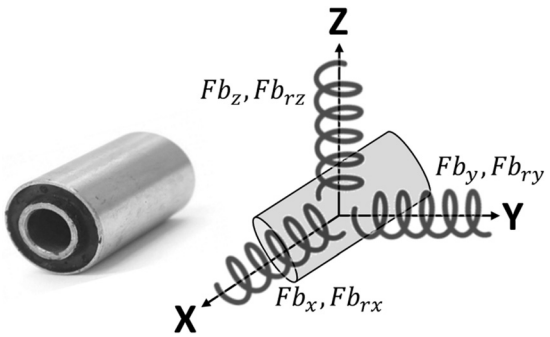

Fig. 2 Bushing model with linear and rotational stiffnesses

To know the vector u, it is necessary to solve a system of N equations, where N depends on the number of elements (9).

$$N = 6 \cdot N_{\text{rigid element}} + 7 \cdot N_{\text{spring rod}} \tag{9}$$

On each rigid element is possible to apply an external force on any point of the body. It is necessary to define a vector $Fext_i$ (10) and its application point $XFext_i$.

$$Fext_i = [Fext_x\, Fext_y\, Fext_z\, Mext_x\, Mext_y\, Mext_z] \tag{10}$$

3 Solving Algorithm and Equations

3.1 Newton–Raphson Solving Algorithm. To solve the equation $f(U) = 0$ a Newton–Raphson method (11) for multiple equation has been used to manage the nonlinearity of the equations. This method is iterative, and the solution is accepted when $\max(\text{abs}(f(U)))$ is less than ε which a small number

$$U_{\text{iter}+1} = U_{\text{iter}} - [J(U_{\text{iter}})]^{-1} \cdot f(U_{\text{iter}}) \tag{11}$$

where $U_0 = [0\,0 \ldots 0]$ and $[J(U_{\text{iter}})]$ is the Jacobian matrix (12) of the function $f(U)$ calculated in U_{Iter}.

$$[J] = \begin{pmatrix} \dfrac{\partial f_1(U)}{\partial U_1} & \cdots & \dfrac{\partial f_1(U)}{\partial U_N} \\ \vdots & \ddots & \vdots \\ \dfrac{\partial f_N(U)}{\partial U_1} & \cdots & \dfrac{\partial f_N(U)}{\partial U_N} \end{pmatrix} \tag{12}$$

The Newton–Raphson algorithm works well if the solution is sufficiently close to the initial condition. For this reason, it may happen that the solver does not converge, particularly in cases where there are high forces or low stiffnesses. One way to overcome this problem has been to break the resolution algorithm into multiple iterations, progressively increasing the vector of external forces. As an example, the code describing the Newton–Raphson algorithm used in this work is shown in Fig. 3. The code is given both in the MATLAB language and in Python. It is particularly noticeable how the function f is also a function of external forces and how the algorithm is broken into three iterations (in this example) to ensure that for each iteration the solution is not too far from the starting point.

3.2 General Equations. The function $f(U)$ is a set of N functions, same dimensions of the displacement vector U.

3.2.1 External Equilibrium Equation. The first six functions (13) and (14) represent the equilibrium equation of the system where the external forces and moments must be equal to the constraint reaction generated by the bushings which is attached to the ground and by the axial reaction of the spring rod element which has one of the bushings attached to the ground.

$$f = \sum Fext[1:3] - \sum Fb_{\text{Chassis}}[1:3](ub) \tag{13}$$

$$f = \sum Fext[4:6] + \sum Fext[1:3] \times XFext - \sum Fb_{\text{Chassis}}[4:6] - \sum Fb_{\text{Chassis}}[1:3](ub) \times Xb \tag{14}$$

3.2.2 Internal Equilibrium Equation. The next functions (15) and (16), on the other hand, describe the also kinematic constraints of the system, considering the stiffness of the bushings which is not attached to the ground and the stiffness of the springs.

A set of six functions is written for each bushing that connects two different elements, so a bushing not constrained to the frame. The functions calculate the difference between the reaction force of the *internal* bushing and the resultant of the forces and moments calculated around the bushing, of one of the two elements chosen arbitrarily.

$$f = \sum Fb[1:3](ub) - Fb_{\text{Int}}[1:3](ub) \tag{15}$$

$$f = \sum Fb[4:6](ub) + \sum Fb_{\text{Int}}[1:3](ub) \times (X - X_{\text{Int}}) - Fb[4:6](ub) \tag{16}$$

Fb_{Int} and X_{Int} represents the reaction forces and position of the bushing that connects the two elements, Fb represents the forces vector of the other bushings of the chose element. The deformation vector ub and the force vector fb are in the local reference system of the bushing. It is therefore necessary to first calculate the appropriate relative deformations of the bushings in the GRS and then operate using the rotation matrices as described in Eq. (2).

3.2.3 Axial Stiffness Equilibrium. Finally, the lasts functions (17) must be written to consider the axial stiffness of the spring rod elements. For each spring rod element, the function is written to calculate the difference between the axial force generated by the spring and the modulus of the reaction force vector of one of the two bushings of the element. For convenience, it is best to choose the bushing whose displacement vector ub also describes the displacement u of the element.

$$f = \|Fb(ub[1:3])\| - Fa(ua) \tag{17}$$

To consider the steering of the suspension by, for example, moving the frame side point of an element representing the trackrod, it is necessary to introduce a displacement vector $dRack$ that is used to

```
iter=3
dim=32
dx=10^-7
J=zeros(dim)
u=zeors(dim,1)
f1 = f(u,Fext/iter);
for i=1:iter
    error=1;
    while error>10^-5
        for k=1:dim
            u(k)= u(k)+dx;
            f2=f(u,Fext*i/iter);
            J(:,k)=(f2-f1)./dx(k);
            u(k)= u(k)-dx;
        end
        u=u-J^-1*f1;
        f1 = f(u,Fext*i/iter);
        error=max(abs(f1));
    end
end
```

```
import numpy as np
iter = 3
dim = 32
dx = 1e-7
J = np.zeros((dim, dim))
u = np.zeros(dim)
f1 = f(u, Fext / iter)
for i in range(1, iter + 1):
    error = 1
    while error > 1e-5:
        for k in range(dim):
            u[k] += dx
            f2 = f(u, Fext * i / iter)
            J[:, k] = (f2 - f1) / dx
            u[k] -= dx
        u = u - np.linalg.solve(J, f1)
        f1 = f(u, Fext * i / iter)
        error = np.max(np.abs(f1))
```

Fig. 3 Code describing the Newton–Raphson algorithm. On the left in MATLAB code, on the right in Python code.

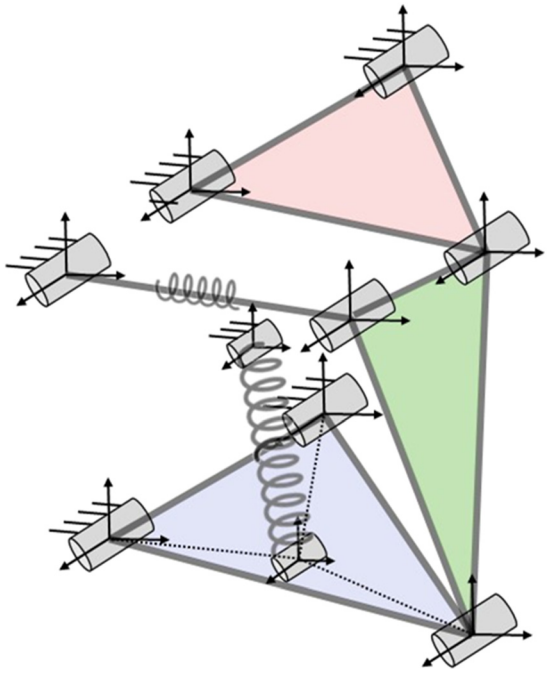

Fig. 4 Double Wishbone suspension scheme used in this work. "Spring rod" for trackrod and spring. "Rigid element" for upper arm, lower arm, and upright.

translate the X vector that describes the position of the bushing in the equations.

At this point, having written the equations as a function of the displacements u that describe the position and rotation of the elements in space and the axial deformations ua, it is possible to apply the solving algorithm to find the solution that represents the deformed configuration of the suspension.

3.3 Double Wishbone Suspension Example. The equations described earlier were written in a very general way on purpose. For a better understanding of the method, it was therefore decided to build an example suspension and the equations for solving the elastokinematics of this configuration will be described below.

A double wishbone front suspension was chosen. The two wishbones were modeled with *rigid elements*, as was the hub carrier. The trackrod was modeled with a *spring rod* element to also provide axial compliance. The spring was also modeled with a *spring rod* that connects the frame to the lower arm. The suspension scheme can be seen in Fig. 4.

The elements are connected to each other and to the frame through deformable bushings. For compactness, we will call the names of the bushings that make up the suspension with acronyms: The front and rear bushings on chassis side of the upper arm are UAFc and UARc, respectively. UAw is the bushing of the upper arm on wheel side. For the lower arm, the bushing's names are LAFc, LARc, and LAw. For the trackrod, the names are TRc and TRw chassis side and wheel side, respectively, and for the spring bushing the names are Sc and Sw. The external forces and moments are applied only in $xFext$ which is a point belonging to the rigid element that describes the upright. For the elements, the upper and lower arm is called UA and LA , respectively, TR, S, and UP for trackrod, spring and upright. WC is the wheel center.

This suspension is modeled with three *rigid element*s and two *spring rods* for a total of $3 \cdot 6 + 2 \cdot 7 = 32$ degrees-of-freedom. U is a 32×1 vector and the number of equations to solve is 32. These equations are reported below creating the function $f(U)$ which will subsequently be set equal to zero to find the solution of the system.

For simplicity of writing, we will establish that in the subsequent equations each ub and Fb vector is referred to in the GRS. However, we know that the Fb function is defined in its local reference system as a function of the displacement vector ub, also defined in LRS. So, only in the writing of the equations below, the change of reference system described in Eq. (2) is omitted to make them more readable.

3.3.1 External Equilibrium for Double Wishbone. The first six functions represent the total equilibrium of the system. The first three (18) functions calculate the difference between the external forces and the reaction forces of the bushings which is attached to the chassis

$$f[1:3] = Fext[1:3] - \sum_j Fb_j[1:3]\left(ub_j[1:3]\right) \tag{18}$$

The fourth to sixth function (19) calculate the difference between the moments generated by the external loads and the moments generated by the bushings on the chassis side

$$f[4:6] = Fext[4:6] - Fext[1:3] \times XFext - \sum_j Fb_j[4:6]\left(ub_j[4:6]\right) + \sum_j Fb[1:3]\left(ub_j[1:3]\right) \times Xb_j \tag{19}$$

where $j = \{UAFc,\ UARc, LAFc, LARc, TRc, Sc\}$ both for Eqs. (18) and (19).

As mentioned before, f is a function of U which is the vector which contains displacement of the elements u and not function of the bushing's deformation ub. So, it is necessary to redefine ub vectors in function of u. For each element attached to the chassis we set that the associated u vector is equal to one of its bushing's vectors. The chosen one is called *main* bushing (20)–(23). If the element is not constrained to the chassis, this equality cannot be made, and the displacement of the element will be given by the deformation of the bushing added to the displacement and rotation in space of the bushing itself (24) and (25).

$$u_{\mathrm{UA}} = ub_{\mathrm{UAFc}} \tag{20}$$

$$u_{\mathrm{LA}} = ub_{\mathrm{LAFc}} \tag{21}$$

$$u_{\mathrm{TR}} = ub_{\mathrm{TRc}} \tag{22}$$

$$u_S = ub_{Sc} \tag{23}$$

$$u_{UP}[1:3] = ub_{\mathrm{UAw}}[1:3] + Xb^{UA}_{\mathrm{UAw}} - Xb_{\mathrm{UAw}} \tag{24}$$

$$u_{UP}[4:6] = ub_{\mathrm{UAw}}[4:6] + u_{UA}[4:6] \tag{25}$$

The upright is not attached to the chassis and Xb^{UA}_{UAw} represents the new point of the Xb_{UAw} bushing associated with the movement of the upper triangle. The understanding of this term will become clearer in later chapters.

The functions 18 and 19 refer to the vectors in the GRS. It is now necessary to express the ub vectors of the other bushings of the element in terms of the u vector of the element. For each element, a reference system attached to the element is then created, oriented like the GRS, and centered on the main bushing previously chosen in Eqs. (20)–(25) to describe the rotation and translation of the element itself. This reference system is called Element Reference System ERS. M is therefore the transformation matrix (26) associated with ERS, attached to the element, and GRS.

$$[M(Xb,u)] = \begin{bmatrix} & [R(u[4:6])] & & \begin{matrix} Xb[1]+u[1] \\ Xb[2]+u[2] \\ Xb[3]+u[3] \end{matrix} \\ 0 & 0 & 0 & 1 \end{bmatrix} \tag{26}$$

where Xb is the position vector of the *main* bushing and $R(u[4:6])$ is the rotation matrix and describe the rotation of the element (27). In the design configuration it is an identity matrix. In general, the

rotation matrix is defined in a similar way to what is described in Eq. (4) with a *Tait-Bryan* transformation $X_1Z_2Y_3$.

$$[R(u[4:6])] = rotx(u[4]) \cdot \text{rot}z(u[6]) \cdot \text{roty}(u[5]) \tag{27}$$

First, it is necessary to calculate the relative coordinates of the positions of the other bushings of the element in the ERS reference system. The transformation matrix $M0(Xb, 0)$ associated with ERS is then created, centered in Xb but with a null u vector (28)

$$[M0(Xb,0)] = \begin{bmatrix} 1 & 0 & 0 & Xb[1] \\ 0 & 1 & 0 & Xb[2] \\ 0 & 0 & 1 & Xb[3] \\ 0 & 0 & 0 & 1 \end{bmatrix} \tag{28}$$

It is now possible to calculate the relative coordinate Xb^{REL} of each other bushing of the element (29)

$$\begin{bmatrix} Xb[1]^{\text{REL,Element}} \\ Xb[2]^{\text{REL,Element}} \\ Xb[3]^{\text{REL,Element}} \\ 1 \end{bmatrix} = [M0]^{-1} \cdot \begin{bmatrix} Xb[1] \\ Xb[2] \\ Xb[3] \\ 1 \end{bmatrix} \tag{29}$$

For the rigid element the ub bushing chassis side deformations are then expressed as a function of u of the element.

$$ub[1:3] = Xb^{\text{Element}}(u) - Xb \tag{30}$$

$$\text{ub}[4:6] = u[4:6] \tag{31}$$

Equations (30) and (31) are true only for chassis side bushings. The displacement of the part constrained to the element is equal to the deformation of the bushing since the bushing is fixed to the chassis.

The rotational deformation is equal for each bushing in the element. The translational deformations are calculated with the differences with the between the new position of the bushing $Xb^{\text{Element}}(u)$ attached on the element side and the position of the bushing Xb on the fixed side where:

$$\begin{bmatrix} Xb^{\text{Element}}(u)[1] \\ Xb^{\text{Element}}(u)[2] \\ Xb^{\text{Element}}(u)[3] \\ 1 \end{bmatrix} = [M(Xb,u)] \cdot \begin{bmatrix} Xb[1]^{\text{REL,Element}} \\ Xb[2]^{\text{REL,Element}} \\ Xb[3]^{\text{REL,Element}} \\ 1 \end{bmatrix} \tag{32}$$

It is then now possible to write the equations for linking bushing deformations on the chassis with element deformations. For the upper arm

$$[M0_{UA}] = \begin{bmatrix} 1 & 0 & 0 & Xb_{UAFc}[1] \\ 0 & 1 & 0 & Xb_{UAFc}[2] \\ 0 & 0 & 1 & Xb_{UAFc}[3] \\ 0 & 0 & 0 & 1 \end{bmatrix} \tag{33}$$

$$\begin{bmatrix} [Xb^{REL,UA}_{UARc}] \\ 1 \end{bmatrix} = [M0_{UA}]^{-1} \cdot \begin{bmatrix} [Xb_{UARc}] \\ 1 \end{bmatrix} \tag{34}$$

$$[M_{UA}] = \begin{bmatrix} [R(u_{UA})] & [Xb_{UAFc} + u_{UA}] \\ 0 \quad 0 \quad 0 & 1 \end{bmatrix} \tag{35}$$

$$\begin{bmatrix} [Xb^{UA}_{UARc}] \\ 1 \end{bmatrix} = [M_{UA}] \cdot \begin{bmatrix} [Xb^{\text{REL},UA}_{UARc}] \\ 1 \end{bmatrix} \tag{36}$$

It is now possible to calculate the bushing deformation on the chassis side.

$$ub_{UARc}[1:3] = Xb^{UA}_{UARc}(u_{UA}) - Xb_{UARc} \tag{37}$$

$$ub_{UARc}[4:6] = u_{UA}[4:6] = u_{UAFc}[4:6] \tag{38}$$

This procedure is better illustrated in Fig. 5.

The same procedure is carried out for the lower arm

$$\begin{bmatrix} [Xb^{REL,LA}_{LARc}] \\ 1 \end{bmatrix} = [M0_{LA}]^{-1} \cdot \begin{bmatrix} [Xb_{LARc}] \\ 1 \end{bmatrix} \tag{39}$$

$$\begin{bmatrix} [Xb^{LA}_{LARc}] \\ 1 \end{bmatrix} = [M_{LA}] \cdot \begin{bmatrix} [Xb^{REL,LA}_{LARc}] \\ 1 \end{bmatrix} \tag{40}$$

$$ub_{LARc}[1:3] = Xb^{LA}_{LARc}(u_{LA}) - Xb_{LARc} \tag{41}$$

$$ub_{LARc}[4:6] = u_{LA}[4:6] = u_{LAFc}[4:6] \tag{42}$$

For *spring rod* elements, this step is not necessary as you always have only one bushing constrained to the chassis.

3.3.2 Internal Equilibrium for Double Wishbone Elements. The first set of equations is now consistent, and we can move on to the second set. In these equations we will instead consider the "internal" bushing that connects the elements together as described in Eqs. (15) and (16). Regarding the bushing UAw that connects the upper arm to the upright the functions (43) are

$$f[7:12] = [R_{UA}] \cdot Fb_{UAw}([R_{UA}]^T \cdot ub_{UAw}) - TF_{UA} \tag{43}$$

Where TF_{UA} is the vector that contains the total forces and moments calculated in the bushings and generated by one of the elements. In this specific case, the arm was chosen as the element

$$TF_{\text{UA}}[1:3] = Fb_{UAFc}(ub_{UAFc}[1:3]) + Fb_{UARc}(ub_{UARc}[1:3]) \tag{44}$$

$$\begin{aligned} TF_{UA}[4:6] = {} & Fb_{UAFc}(ub_{UAFc}[4:6]) + Fb_{UARc}(ub_{UARc}[4:6]) \\ & + Fb_{UAFc}(ub_{UAFc}[1:3]) \times \left(Xb_{UAFc} - Xb^{UA}_{UAw}\right) \\ & + Fb_{UARc}(ub_{UARc}[1:3]) \times \left(Xb_{UARc} - Xb^{UA}_{UAw}\right) \end{aligned} \tag{45}$$

Xb^{UA}_{UAw} is the new position of the bushing due to the deformation of the upper arm element. It is calculated in the same way of the other bushing in the rigid element (46) and (47).

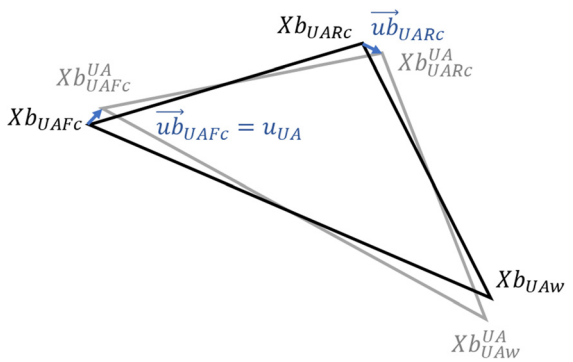

Fig. 5 Upper arm, scheme to identify the chassis side bushing deformations

$$\begin{bmatrix} [Xb^{UA}_{UAw}] \\ 1 \end{bmatrix} = [M_{UA}] \cdot \begin{bmatrix} [Xb^{\mathrm{REL},UA}_{UAw}] \\ 1 \end{bmatrix} \tag{46}$$

$$\begin{bmatrix} [Xb^{\mathrm{REL},UA}_{UAw}] \\ 1 \end{bmatrix} = [M0_{UA}]^{-1} \cdot \begin{bmatrix} [Xb_{UAw}] \\ 1 \end{bmatrix} \tag{47}$$

R_{UA} is the rotation matrix associated with the upper arm (48). Since the *ub* vectors are referential to the GRS, it is necessary to return them to the local reference system since this bushing can rotate in space since it is constrained to the element and not to the frame.

$$[R_{UA}] = rotx(u_{UA}[4]) \cdot rotz(u_{UA}[6]) \cdot roty(u_{UA}[5]) \tag{48}$$

The bushing deformation ub_{UAw}, is

$$ub_{UAw}[1:3] = u_{UP}[1:3] - \left(Xb^{UA}_{UAw} - Xb_{UAw}\right) \tag{49}$$

$$ub_{UAw}[4:6] = u_{UP}[4:6] - u_{UA}[4:6] \tag{50}$$

Other elements of the function f regarding the lower triangle can be written in a similar way (51).

$$f[13:18] = [R_{LA}] \cdot Fb_{LAw}([R_{LA}]^T \cdot ub_{LAw}) - TF_{LA} \tag{51}$$

$$[R_{LA}] = rotx(u_{LA}[4]) \cdot rotz(u_{LA}[6]) \cdot roty(u_{LA}[5]) \tag{52}$$

In this case, the lower triangle is also constrained to the spring through a bushing, so we enter the TF_S vector that accounts for forces and moments generated by the spring.

$$\begin{aligned} TF_{LA}[1:3] = {} & Fb_{LAFc}(ub_{LAFc}[1:3]) + Fb_{LARc}(ub_{LARc}[1:3]) \\ & + TF_S[1:3] \end{aligned} \tag{53}$$

$$\begin{aligned} TF_{LA}[4:6] = {} & Fb_{LAFc}(ub_{LAFc}[4:6]) \\ & + Fb_{LARc}(ub_{LARc}[4:6]) + TF_S[4:6] \\ & + Fb_{LAFc}(ub_{LAFc}[1:3]) \times \left(Xb_{LAFc} - Xb^{LA}_{UAw}\right) \\ & + Fb_{LARc}(ub_{LARc}[1:3]) \times \left(Xb_{LARc} - Xb^{LA}_{UAw}\right) \\ & + TF_S[1:3] \times \left(Xb^{LA}_{Sw} - Xb^{LA}_{UAw}\right) \end{aligned} \tag{54}$$

$$\begin{bmatrix} [Xb^{REL,LA}_{LAw}] \\ 1 \end{bmatrix} = [M0_{LA}]^{-1} \cdot \begin{bmatrix} [Xb_{LAw}] \\ 1 \end{bmatrix} \tag{55}$$

$$\begin{bmatrix} [Xb^{LA}_{LAw}] \\ 1 \end{bmatrix} = [M_{LA}] \cdot \begin{bmatrix} [Xb^{REL,LA}_{LAw}] \\ 1 \end{bmatrix} \tag{56}$$

$$\begin{bmatrix} [Xb^{REL,LA}_{Sw}] \\ 1 \end{bmatrix} = [M0_{LA}]^{-1} \cdot \begin{bmatrix} [Xb_{Sw}] \\ 1 \end{bmatrix} \tag{57}$$

$$\begin{bmatrix} [Xb^{LA}_{Sw}] \\ 1 \end{bmatrix} = [M_{LA}] \cdot \begin{bmatrix} [Xb^{REL,LA}_{Sw}] \\ 1 \end{bmatrix} \tag{58}$$

Everything in Eqs. (53) and (54) is very similar to what we saw in the previous set of Eqs. (44) and (45). The only significative difference is the presence of the term ub_{LAw} representing the deformation of the bushing connecting hub carrier and lower arm.

Again, as always, it is necessary to relate the bushing deformation back to the displacement vector of the element. In this case, to calculate the bushing deformation vector, it will be necessary to know the new position of the bushing constrained on the arm and constrained on the upright. The difference of these two vectors is the translational bushing deformation (59)

$$ub_{LAw}[1:3] = Xb^{UP}_{LAw}(u_{UP}) - Xb^{LA}_{LAw}(u_{LA}) \tag{59}$$

Regarding rotations, the bushing deformation is given by the difference between the rotation of the upright and the rotation of the lower arm (60) because the bushing connects these two elements

$$ub_{LAw}[4:6] = u_{UP}[4:6] - u_{LA}[4:6] \tag{60}$$

Since the upright is a rigid element, the procedure is analogous to that seen for the two wishbones

$$\begin{bmatrix} [Xb^{\mathrm{REL},UP}_{LAw}] \\ 1 \end{bmatrix} = [M0_{UP}]^{-1} \cdot \begin{bmatrix} [Xb_{LAw}] \\ 1 \end{bmatrix} \tag{61}$$

$$\begin{bmatrix} [Xb^{UP}_{LAw}] \\ 1 \end{bmatrix} = [M_{UP}] \cdot \begin{bmatrix} [Xb^{\mathrm{REL},UP}_{LAw}] \\ 1 \end{bmatrix} \tag{62}$$

This procedure to identify the bushing deformation is also explained in the Fig. 6.

For spring rod elements, the axial deformation *ua* of the element must also be considered. Once $\widehat{Xb}^{\mathrm{Element}}_2$ has been calculated through the transformation matrix and the relative coordinates as with what we have already seen for the rigid element. An additional step is needed to calculate the new point Xb^{Element}_2 while also considering axial deformation

$$Xb^{\mathrm{Element}}_2 = \widehat{Xb}^{\mathrm{Element}}_2 + ua \circ cosdir \tag{63}$$

Where $\circ$ is the element-by-element product and *cosdir* is the vector with the cosine directors (64) associated with the axial direction of the *spring rod* element.

$$cosdir_{\mathrm{element}} = \frac{\left(Xb^{\mathrm{Element}}_1 - \widehat{Xb}^{\mathrm{Element}}_2\right)}{\|Xb^{\mathrm{Element}}_1 - \widehat{Xb}^{\mathrm{Element}}_2\|} \tag{64}$$

Xb^{Element}_1 and Xb^{Element}_2 are the new position vector associated with two bushing of the *spring rod* element. This procedure is well described in Fig. 7.

After explaining this procedure, we can then proceed to the calculation of Xb^S_{Sw} (69).

$$Xb^S_{Sc} = Xb_{Sc} + u_S \tag{65}$$

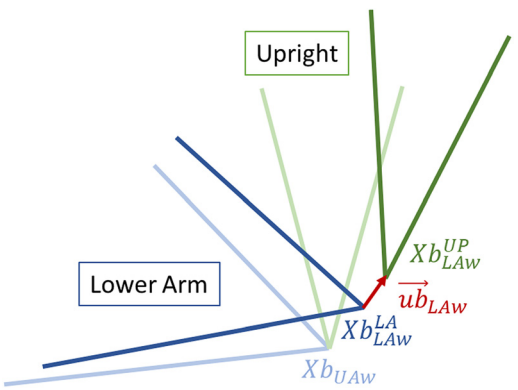

Fig. 6 Lower arm and upright, scheme to identify wheel side bushing deformations

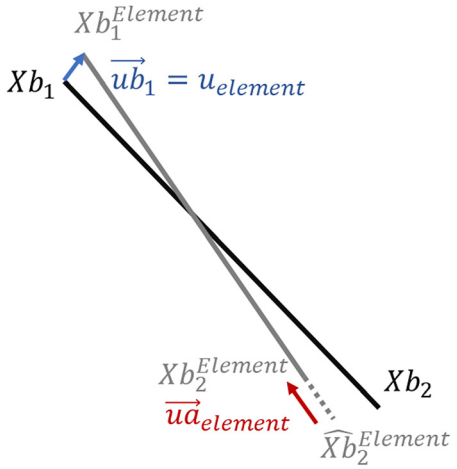

Fig. 7 Spring rod element, scheme to identify bushing deformations with axial displacement

$$\begin{bmatrix} [Xb_{Sw}^{\mathrm{REL},S}] \\ 1 \end{bmatrix} = [M0_S]^{-1} \cdot \begin{bmatrix} [Xb_{Sw}] \\ 1 \end{bmatrix} \tag{66}$$

$$\begin{bmatrix} [\widehat{Xb}_{Sw}^{S}] \\ 1 \end{bmatrix} = [M_S] \cdot \begin{bmatrix} [Xb_{Sw}^{\mathrm{REL},S}] \\ 1 \end{bmatrix} \tag{67}$$

$$cosdir_S = \frac{\left(Xb_{Sc}^{S} - \widehat{Xb}_{Sw}^{S}\right)}{\|Xb_{Sc}^{S} - \widehat{Xb}_{Sw}^{S}\|} \tag{68}$$

$$Xb_{Sw}^{S} = \widehat{Xb}_{Sw}^{S} + ua_S \circ cosdir_S \tag{69}$$

To complete the equations describing the balance of the lower arm, we calculate the vector TF_S (70) and (71).

$$TF_S[1:3] = Fb_{Sc}(ub_{Sc}[1:3]) \tag{70}$$

$$\begin{aligned} TF_S[4:6] = {} & Fb_{Sc}(ub_{Sc}[4:6]) + Fb_{Sc}(ub_{Sc}[1:3]) \\ & \times \left(Xb_{Sc}^{S} - Xb_{Sw}^{S}\right) \end{aligned} \tag{71}$$

It is now possible to write the new set of functions of f to describe the equilibrium on the bushing connecting the spring with the lower arm (72).

$$f[19:24] = [R_{LA}] \cdot Fb_{Sw}\left([R_{LA}]^T \cdot ub_{Sw}\right) - TF_S \tag{72}$$

Where

$$ub_{Sw} = Xb_{Sw}^{S}(u_S, ua_S) - Xb_{Sw}^{LA}(u_{LA}) \tag{73}$$

The steering tie rod is now considered. The procedure is quite similar to what has already been seen. However, the possibility of moving the chassis-side bushing along the y-axis to simulate the translation of the rack is considered. So, a new vector $dTRc$ is considered (74)

$$dTRc = \begin{bmatrix} 0 \\ dRack \\ 0 \\ 0 \\ 0 \\ 0 \end{bmatrix} \tag{74}$$

Where dRack is the rack displacement. The new set of functions associated with the trackrod attached to the upright is reported below (75).

$$f[25:30] = [R_{TR}] \cdot Fb_{TRw}\left([R_{TR}]^T \cdot ub_{TRw}\right) - TF_{TR} \tag{75}$$

Where R_{TR} is the rotation matrix associated with the trackrod element displacement u_{TR}. ub_{TRw} is expressed in Eqs. (76) and (77)

$$ub_{TRw}[1:3] = Xb_{TRw}^{UP}(u_{UP}) - Xb_{TRw}^{TR}(u_{TR}, ua_{TR}) \tag{76}$$

$$ub_{TRw}[4:6] = u_{UP}[4:6] - u_{TR}[4:6] \tag{77}$$

$$\begin{bmatrix} [Xb_{TRw}^{\mathrm{REL},UP}] \\ 1 \end{bmatrix} = [M0_{UP}]^{-1} \cdot \begin{bmatrix} [Xb_{TRw}] \\ 1 \end{bmatrix} \tag{78}$$

$$\begin{bmatrix} [Xb_{TRw}^{UP}] \\ 1 \end{bmatrix} = [M_{UP}] \cdot \begin{bmatrix} [Xb_{TRw}^{REL,UP}] \\ 1 \end{bmatrix} \tag{79}$$

like the spring, but also considering the rack displacement:

$$Xb_{TRc}^{TR} = Xb_{TRc} + u_{TR} + dTRc \tag{80}$$

$$\begin{bmatrix} [Xb_{TRw}^{\mathrm{REL},TR}] \\ 1 \end{bmatrix} = [M0_{TR}]^{-1} \cdot \begin{bmatrix} [Xb_{TRw}] \\ 1 \end{bmatrix} \tag{81}$$

$$\begin{bmatrix} [Xb_{TRw}^{TR}] \\ 1 \end{bmatrix} = [M_{TR}] \cdot \begin{bmatrix} [Xb_{TRw}^{REL,TR}] \\ 1 \end{bmatrix} \tag{82}$$

$$cosdir_{TR} = \frac{\left(Xb_{TRc}^{TR} - \widehat{Xb}_{TRw}^{TR}\right)}{\|Xb_{TRc}^{S} - \widehat{Xb}_{TRw}^{S}\|} \tag{83}$$

$$Xb_{TRw}^{TR} = \widehat{Xb}_{TRw}^{TR} + ua_{TR} \circ cosdir_{TR} \tag{84}$$

$M0_{TR}$ is calculated similarly to all other elements. The matrix M_{TR}, on the other hand, is calculated by also considering the frame-side bushing translation given by the steering (85).

$$[M_T] = \begin{bmatrix} & [R(u_{TR})] & & [Xb_{TRc} + u_{TR} + dTRc] \\ 0 & 0 & 0 & 1 \end{bmatrix} \tag{85}$$

To conclude this set of equations, we also define the force vector TF_{TR} (86) and (87).

$$TF_{TR}[1:3] = Fb_{TRc}(ub_{TRc}[1:3]) \tag{86}$$

$$\begin{aligned} TF_{TR}[4:6] = {} & Fb_{TRc}(ub_{TRc}[4:6]) \\ & + Fb_{TRc}(ub_{TRc}[1:3]) \\ & \times \left(Xb_{TRc}^{S} + dTRc[1:3] - Xb_{TRw}^{S}\right) \end{aligned} \tag{87}$$

3.3.3 Equilibrium for Spring Rod Double Wishbone's Element. Finally, to complete the function f we need to define the last two functions (88) and (89). These take into account the axial stiffness of the spring and the trackrod.

$$f(31) = \|Fb_{Sc}(ub_{Sc}[1:3])\| - Fa_S(ua_S) \tag{88}$$

$$f(32) = \|Fb_{TRc}(ub_{TRc}[1:3])\| - Fa_{TR}(ua_{TR}) \tag{89}$$

Where $ub_{Sc} = u_S$ and $ub_{TRc} = u_{TR}$.

Now that the function f is totally defined, it is possible to calculate the displacement vector U describing the deformed configuration of

the suspension by means of the Newton–Raphson algorithm described earlier in Eq. (11).

4 Model Comparison With Multibody

All equations, including the function and solving algorithm were implemented in MathWorks Matlab®. The suspension pickup points are reported in Table 1. It is specified that this is not a real suspension but only a model created for demonstration purposes for this work.

The reference system in question is a right-handed system, originating in the center of the front axle. The *X*-axis faces in the forward direction of the vehicle and the *Z*-axis faces upward.

For the comparison, the same suspension has been designed using MathWorks Simscape® Multibody with the same pickup points, same bushing, and same forces (Fig. 8). It is not the purpose of this paper to explain how the suspension model was recreated on this software.

Being a multibody software, the simulation also takes inertial and damping effects into account. For this reason, only the last values are taken as useful data for comparison, once the transient is exhausted and the whole system is at steady-state, equilibrium is given only by the stiffnesses. For simplicity, in the design configuration all bushings are oriented the same way and in particular the local axes of each bushing are oriented as the axes of the GRS.

Unfortunately, Simscape® does not allow modeling of bushing with nonlinear stiffnesses. it is only possible to assign six stiffness values for each bushing and one axial stiffness. Therefore, linear stiffnesses are used for both bushing and axial compliance for models comparison purposes.

All frame-side bushings have the same stiffnesses, and their values are given in Table 2. Same for wheel-side bushing, which are all the same and have the same translational stiffnesses as frame-side bushing but one-tenth the rotational stiffness. This is to avoid making the suspension too stiff during steering. It should be noted that again the stiffness values do not represent actual bushing, although an order of magnitude consistent with commercially available bushing is chosen

Table 3 shows the general characteristics of the vehicle on which this idealized front suspension is mounted. The vehicle data are used to calculate the load cases that will be used later for the comparison.

Table 4 shows the load cases used to compare the model with the reference. Ten cases were chosen, containing braking, acceleration, lateral, and combined loads. The last two load cases, on the other hand, want to recreate the suspension hitting a pothole while braking and the wheel hitting a curb sideways.

The load cases are defined as three forces and three moments applied on the hub carrier. Loads were calculated by considering vehicle data and load transfers given by accelerations. It is not the purpose of this paper to report the equations by which the loads were obtained. The points of load application vary according to the case and are given in Table 5 with the translation of the rack.

Figure 9 show the schematic of the suspension in the design configuration and the deformed configuration after applying load case number 4 and 7, as an example. Two views of the suspension are shown in the figures, and the deformed configuration calculated through the model and that calculated through Simscape® is shown.

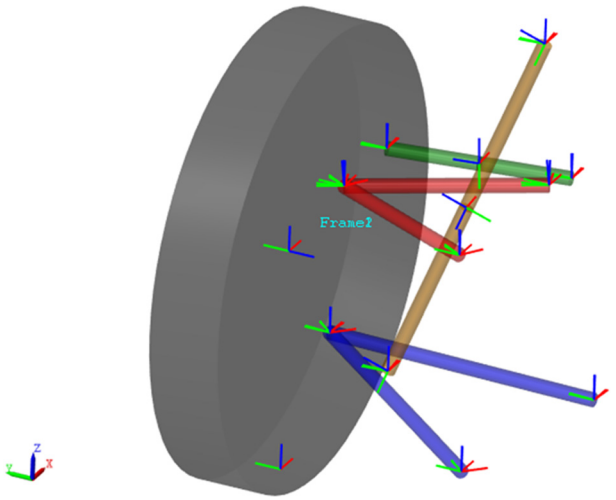

Fig. 8 Suspension model designed in Simscape® Multibody

Table 2 Bushings translational and rotational stiffness

	K_x $\left(\frac{N}{mm}\right)$	K_y $\left(\frac{N}{mm}\right)$	K_z $\left(\frac{N}{mm}\right)$	Kr_x $\left(\frac{Nm}{deg}\right)$	Kr_y $\left(\frac{Nm}{deg}\right)$	Kr_z $\left(\frac{Nm}{deg}\right)$
UAFc	1000	2000	3000	1500	30000	30000
UARc	1000	2000	3000	1500	30000	30000
UAw	1000	2000	3000	150	3000	3000
LAFc	1000	2000	3000	1500	30000	30000
LARc	1000	2000	3000	1500	30000	30000
LAw	1000	2000	3000	150	3000	3000
TRc	1000	2000	3000	1500	30000	30000
TRw	1000	2000	3000	150	3000	3000
Sc	1000	2000	3000	1500	30000	30000
Sw	1000	2000	3000	150	3000	3000

To do the comparison, we chose to compare the values describing the position is the orientation of the wheel in space in the deformed configuration. Specifically, Tables 6 and 7 show the changes from the design configuration of the wheel center coordinates and rotations about their axes, namely, camber, toe and side view angle (SWA). Table 6 shows the calculation result of the model, and Table 7 shows the calculation result of Simscape®.

Table 8 shows the normalized root mean squared error (nRMSE) and the Pearson correlation coefficient (R) values calculated by the model compared with those calculated with Simscape®.

The results shown in Table 8 are also shown in the graphs in Fig. 10 for better visualization.

Table 1 Suspension pickup points coordinates

	X (mm)	*Y* (mm)	*Z* (mm)
UAFc	50	400	480
UARc	−180	420	470
UAw	−30	660	450
LAFc	0	300	210
LARc	−300	350	220
LAw	30	700	200
TRc	120	400	460
TRw	100	660	450
Sc	20	400	700
Sw	0	600	180
WC	0	750	320

Table 3 Vehicle characteristics used for load cases calculation

Wheelbase (mm)	2750
Front track (mm)	1500
Rear track (mm)	1500
CG height (mm)	500
Traction	RWD
Total mass (kg)	1600
Total weight distribution (%)	60
Nonsuspended mass front (kg)	80
Nonsuspended mass rear (kg)	80
Roll stiffness distribution (%)	60
Wheel radius (mm)	320
Braking forces distribution (%)	65
Pneumatic trail (mm)	20

Table 4 List of load cases used for the comparison

N	Load case	F_x (N)	F_y (N)	F_z (N)	M_x (Nm)	M_y (Nm)	M_z (Nm)
1	Static weight	0	0	4709	0	0	0
2	Static weight * 1.5 g	0	0	7063.5	0	0	0
3	Braking 0.5 g	−2550.6	0	5422	0	0	0
4	Braking 0.8 g	−4080.96	0	5850	0	0	0
5	Acceleration 0.4 g	3139.2	0	4138	0	0	0
6	Cornering 0.7 g	0	−4630	6867	0	0	92.6
7	Corn 0.7 g+ Acc 0.4 g	3139.2	−4630	4345	0	1004.544	92.6
8	Corn 0.7 g+ Brk 0.8 g	−4080.96	−4630	8009	0	0	92.6
9	Pothole braking	−8161.92	0	7563	0	0	0
10	Curb sideways	0	−7500	4709	0	0	0

Note: "*" indicates multiplication

Table 5 Forces application points and rack displacement for each load cases

N	Load case	X	Y (mm)	Z (mm)	dRack (mm)
1	Static weight	0	750	0	0
2	Static weight * 1.5 g	0	750	0	0
3	Braking 0.5 g	0	750	0	0
4	Braking 0.8 g	0	750	0	0
5	Acceleration 0.4 g	0	750	320	0
6	Cornering 0.7 g	0	750	0	−20
7	Corn 0.7 g+ Acc 0.4 g	0	750	0	−20
8	Corn 0.7 g+ Brk 0.8 g	0	750	0	−20
9	Pothole braking	0	750	0	0
10	Curb sideways	0	750	200	0

Note: "*" indicates multiplication

5 Non-Linear Bushings and Suspension Element Analysis

This chapter reports the results of elastokinematics computations using nonlinear bushings, spring and trackrod. The same suspension scheme seen in the previous chapter is used, with the same pickup points. However, nonlinear stiffnesses are used to better simulate the true behavior of bushing. Specifically, each of the six force–displacement functions that characterize bushing are described by the function $Fb_{NL}(ub)$. Each of these functions is described by a fifth-degree polynomial with a first-degree term inside to describe the linear behavior for small displacements. The shape of the function is graphed in Fig. 11. Displacements and rotations are defined in millimeters and radians.

$$Fb_{NL}(ub) = (ub \circ cx)^{\circ 5} + 1000 \cdot \mathrm{cx} \circ ub) \circ cy \tag{90}$$

Where, for the bushings, the coefficients cx and cy are two 6x1 vectors associated with each of the six bushing stiffnesses. All bushings are oriented as described in the previous chapter, and the rotational stiffnesses of the wheel-side bushings are one-tenth of those on the chassis-side as can be seen from in Eqs. (91)–(93).

$$cx_c = cx_W = \begin{bmatrix} 1 & 1 & 1 & 180/\pi & 180/\pi & 180/\pi \end{bmatrix} \tag{91}$$

$$cy_c = \begin{bmatrix} 1\mathrm{N} & 2\mathrm{N} & 3\mathrm{N} & 1.5\mathrm{Nmm} & 30\mathrm{Nmm} & 30\mathrm{Nmm} \end{bmatrix} \tag{92}$$

$$cy_w = \begin{bmatrix} 1\mathrm{N} & 2\mathrm{N} & 3\mathrm{N} & 1.5\mathrm{Nmm} & 30\mathrm{Nmm} & 30\mathrm{Nmm} \end{bmatrix} \tag{93}$$

The axial stiffness of the trackrod (94) is also defined by a similar function of (90) where $cx_{TR} = 1$ and $cy_{TR} = 5$.

$$Fa_{TR}(ua_{TR}) = (ua_{TR})^5 + 1000 \cdot ua_{TR}) \cdot 5N \tag{94}$$

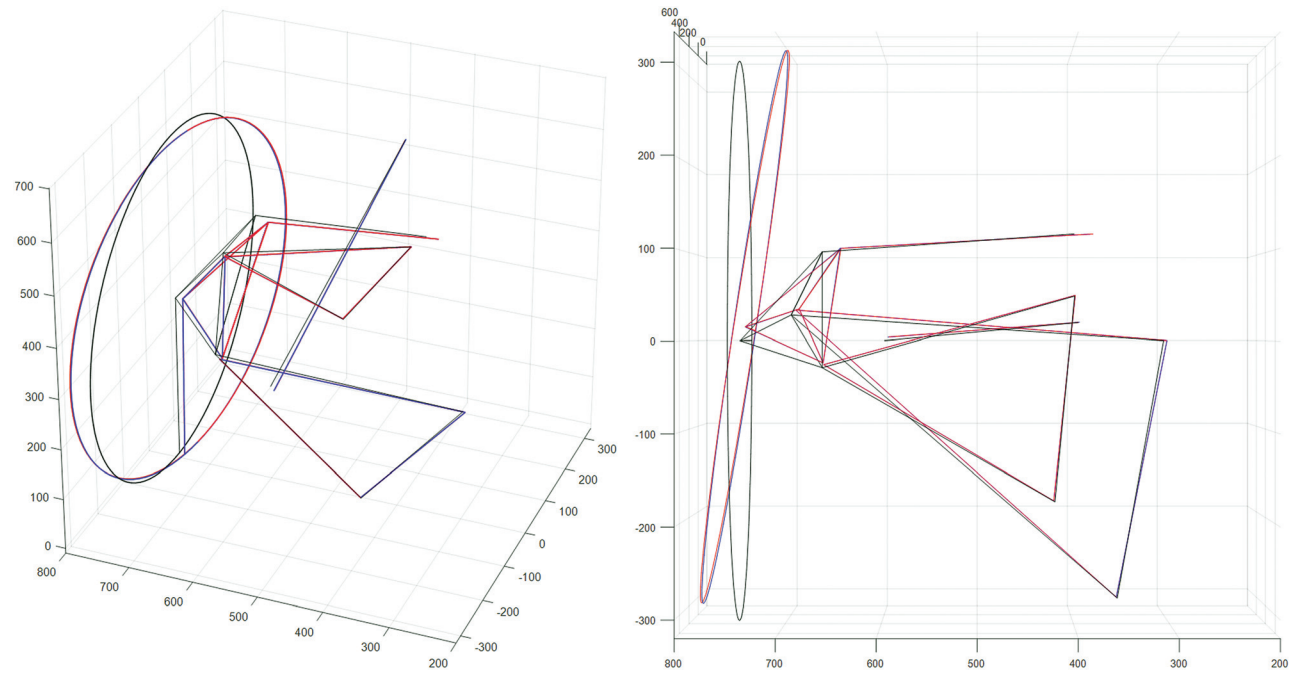

Fig. 9 Graphic view of the deformed suspension under load number 7. Design configuration (black), model deformed configuration (red), Simscape® (blue).

Table 6 Calculation results of the model for each load case

N	dCamber(deg)	dSWA(deg)	*dToe*(deg)	*dX*(mm)	*dY*(mm)	*dZ*(mm)
1	−0.75	−1.33	0.28	−1.28	1.57	4.69
2	−1.21	−1.16	1.82	−0.52	−0.95	69.41
3	−1.49	−5.72	0.15	−6.42	3.54	22.07
4	−1.98	−8.33	−0.05	−9.73	4.23	33.04
5	−0.63	−1.26	1.26	4.02	0.40	−9.18
6	−0.91	−1.04	9.00	11.76	−6.71	70.52
7	−0.17	−0.77	8.16	16.10	−5.11	−9.38
8	−2.14	−8.50	6.33	−1.16	−11.86	109.51
9	−3.80	−15.32	−1.39	−20.33	1.84	80.44
10	0.99	0.00	−1.68	−0.57	−5.27	−17.45

Table 7 Calculation result of Simscape® model for each load case

N	dCamber (deg)	dSWA (deg)	dToe (deg)	*dX* (mm)	*dY* (mm)	*dZ* (mm)
1	−0.75	−1.32	0.28	−1.27	1.59	4.97
2	−1.22	−1.14	1.83	−0.57	−1.00	69.84
3	−1.48	−5.62	0.11	−6.43	3.50	22.27
4	−1.96	−8.17	−0.12	−9.75	4.16	33.09
5	−0.63	−1.27	1.27	4.04	0.44	−8.90
6	−0.80	−0.95	8.49	11.05	−6.57	70.27
7	−0.11	−0.75	7.84	15.68	−5.10	−9.88
8	−2.02	−8.17	5.90	−1.70	−11.25	107.61
9	−3.74	−14.91	−1.52	−20.27	1.98	78.52
10	1.02	0.03	−1.89	−0.85	−5.36	−18.23

Instead, the spring is described in Eq. (95) with a linear function and preload. However, the presence of a bumpstop with a clearance. The curve force–displacement of the bumpstop is analogous to Eq. (90).

$$Fa_S(ua_S) = \begin{cases} k_s \cdot ua_s N, \; ua_s < clr \\ k_s \cdot ua_s + ((ua_S - clr)^5 + 1000 \cdot (ua_s - clr)) \cdot 0.2\,N, \; ua_s \geq clr \end{cases} \tag{95}$$

where $k_s = 60\,\mathrm{N/mm}$ is the spring stiffness and $\mathrm{clr} = 40\,\mathrm{mm}$ is the bumpstop clearance.

These displacement force curves were chosen to make sure that for small displacements the suspension has stiffnesses quite similar to the one analyzed in the previous chapter. Next, in fact, a comparison is made between the model with linear and nonlinear stiffnesses to understand how much the nonlinearity can affect the suspension deformation. We chose to compare them using probably what is the heaviest load case, number 8 expressed in Table 4. The schematic of the deformed suspension is shown in Fig. 12 and forces and moments generated by one of the bushings are shown instead in Fig. 13. The rear bushing of the lower arm was chosen as an example.

Finally, the wheel motion was chosen to be observed to see the evolution of elastokinematics at various fractions of the load case. Always using load number 8 defined in Table 4, the calculation is carried out ten times starting first from 10% of the load, then 20% and so on until it reaches 100%. In addition to loads, rack displacement and spring preload are also made to vary progressively. The translations and rotations of the wheel center are shown in Fig. 14. Comparing the suspension with linear and nonlinear stiffnesses.

Table 8 Normalized root mean squared error and *R* between model and Simscape® results

	dCamber (deg)	dSWA (deg)	dToe (deg)	*dX* (mm)	*dY* (mm)	*dZ* (mm)
nRMSE (%)	3.7%	2.9%	5.9%	3.3%	4.0%	1.7%
R	0.999	1.000	0.999	1.000	1.000	1.000

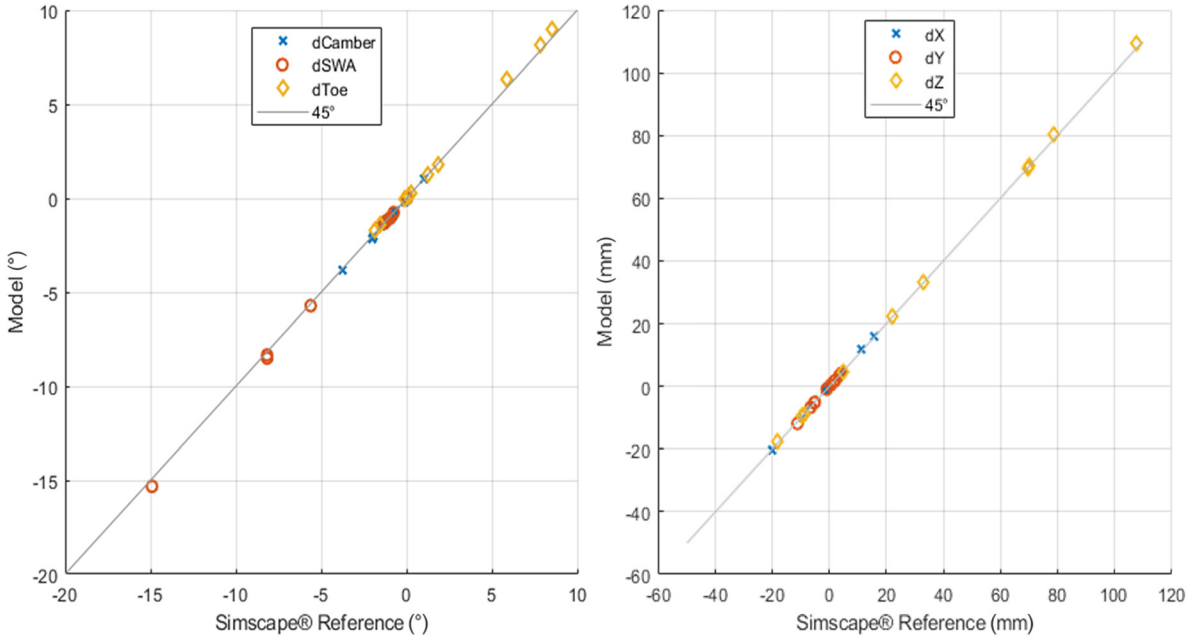

Fig. 10 Model results versus Simscape® results. Wheel orientation (dCamber, dSWA, dToe) on the left side and position (*dX*, *dX*, *dZ*) on the right side

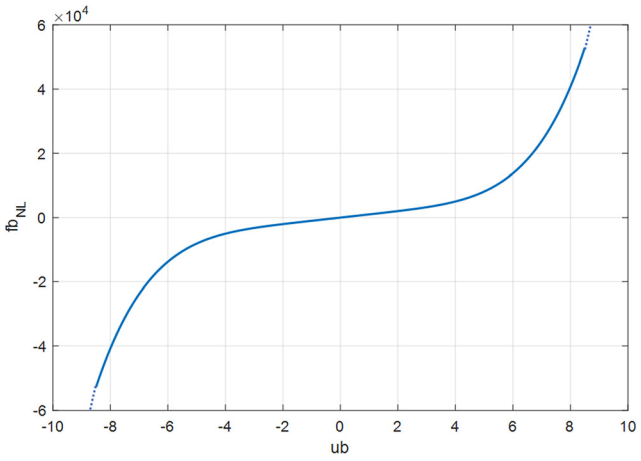

Fig. 11 Shape of the function (90), on *X*-axis the bushing deformation, on *Y*-axis per bushing reaction

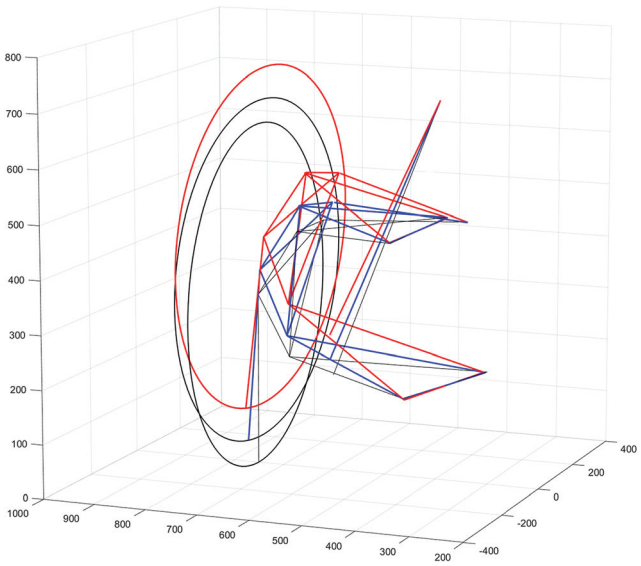

Fig. 12 Graphic view of the deformed suspension both for linear and nonlinear model under the load N8. Design configuration (black), linear (red), and nonlinear (blue)

6 Sensitivity Analysis

In this chapter, a sensitivity analysis is given as an example. The first objective is to show how modeling bushing nonlinearities can affect the parameters of the suspension and thus its performance. The second objective is to explore the ease with which a sensitivity analysis can be performed, thanks to the parameterization of the code. The usual double wihsbone suspension described in the previous chapters is taken, the spring is placed of infinite stiffness so that only the contribution of the bushing on the elastokinematics can be isolated and movements due to the suspension kinematics can be excluded. Force-displacement curves are described as Eq. (90). A number K that multiplies only the chassis-side bushing stiffness curve has been chosen as a parameter for the sensitivity analysis (96)

$$Fb_{\text{Chassis}}(ub) = K \cdot (ub \circ cx)^{\circ 5} + 1000 \cdot \text{cx} \circ ub) \circ cy \qquad (96)$$

The parameter K, which then scales the force–displacement curve, is varied with values ranging from 0.4 to 2, with a step of 0.2. The different force–displacement curves obtained as K changes are then shown in Fig. 15.

As an example, it is chosen to show how the Camber and Track values vary when the parameter K is varied and when a force Fx is varied from -7000 N to $+7000$ N.

Some results of the sensitivity analysis are depicted in Fig. 16 showing the surfaces representing the variations of Camber and Track as a function of force Fx and parameter K.

In this straightforward example, the different modeling of the bushing characteristic curve influences the elasto-kinematic characteristics of the suspension. In it can be even seen an inversion of the sign of the track compliance in Fig. 16.

7 Conclusion

A model for computing the elastokinematics of a suspension was developed. Reviewing the literature, it was found to be one of the most comprehensive, due to the fact that it takes into account mainly nonlinear stiffnesses and the possibility of using wheel-side bushings as well. In addition, the calculation is done iteratively and takes into account the kinematics of the suspension, unlike many works that simply calculate the stiffness matrix of the system, which is practically useless when large deformations occur. As seen in the last chapter, considering stiffnesses as linear can only be a sensible approximation for small loads and small displacements. The mathematical model is capable not only of calculating the deformed configuration of the suspension, but also of returning the constrained reactions on each bushing of the suspension. This is useful for suspension design process as an input to FEM models.

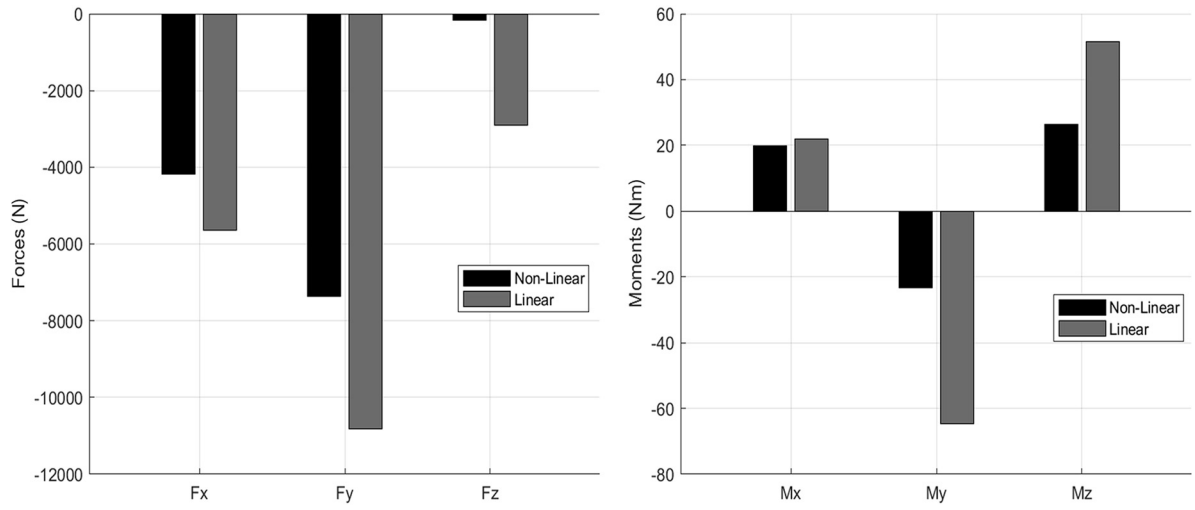

Fig. 13 Forces (left) and moments (right) of the lower arm rear bushing under the load case N8

Compared with a model created using multibody software, the computation time is essentially negligible; code written in Matlab® takes one or two tenths of a second to converge to the solution. The model has also proven to be particularly useful just to perform kinematic analysis of the suspension by appropriately modifying the stiffness of the bushings and elements. Once it is understood how to write the equations depending on how the various elements are linked together, any type of independent-wheel suspension can be created. This makes this model particularly powerful in developing the elastokinematics of suspension quickly. In fact, the force–displacement curves that characterize bushings and elements can also be changed easily as a key feature in the design phase. The presented methodology proved to be particularly effective, especially for the possibility of handling the nonlinear force-deformation curves of the joints. Most models in the literature do not consider these effects, but they make a substantial difference, as can be seen from Figs. 14 and 15. Designing suspension compliance correctly can have macroscopic effects, both on driving feel and vehicle balance, with implications for safety and performance as well.

It can be stated that this algorithm represents a kind of virtual K&C. Having a validated model can lead, at an early stage of the design, to saving time and money spent at a test bench. In addition, several combinations of forces and moments can be tested through simulations that are difficult to achieve with a K&C test rig. As this method has a high computing speed, it can be combined with optimization or sensitivity analysis algorithms to speed up the design process as much as possible. For example, having a function written in Matlab®, it is possible to use the proprietary "Optimization Toolbox" with relative ease. Having a fully parameterized algorithm makes it easy to perform sensitivity analyses as in Chapter 6. Another application the author is working on is the use

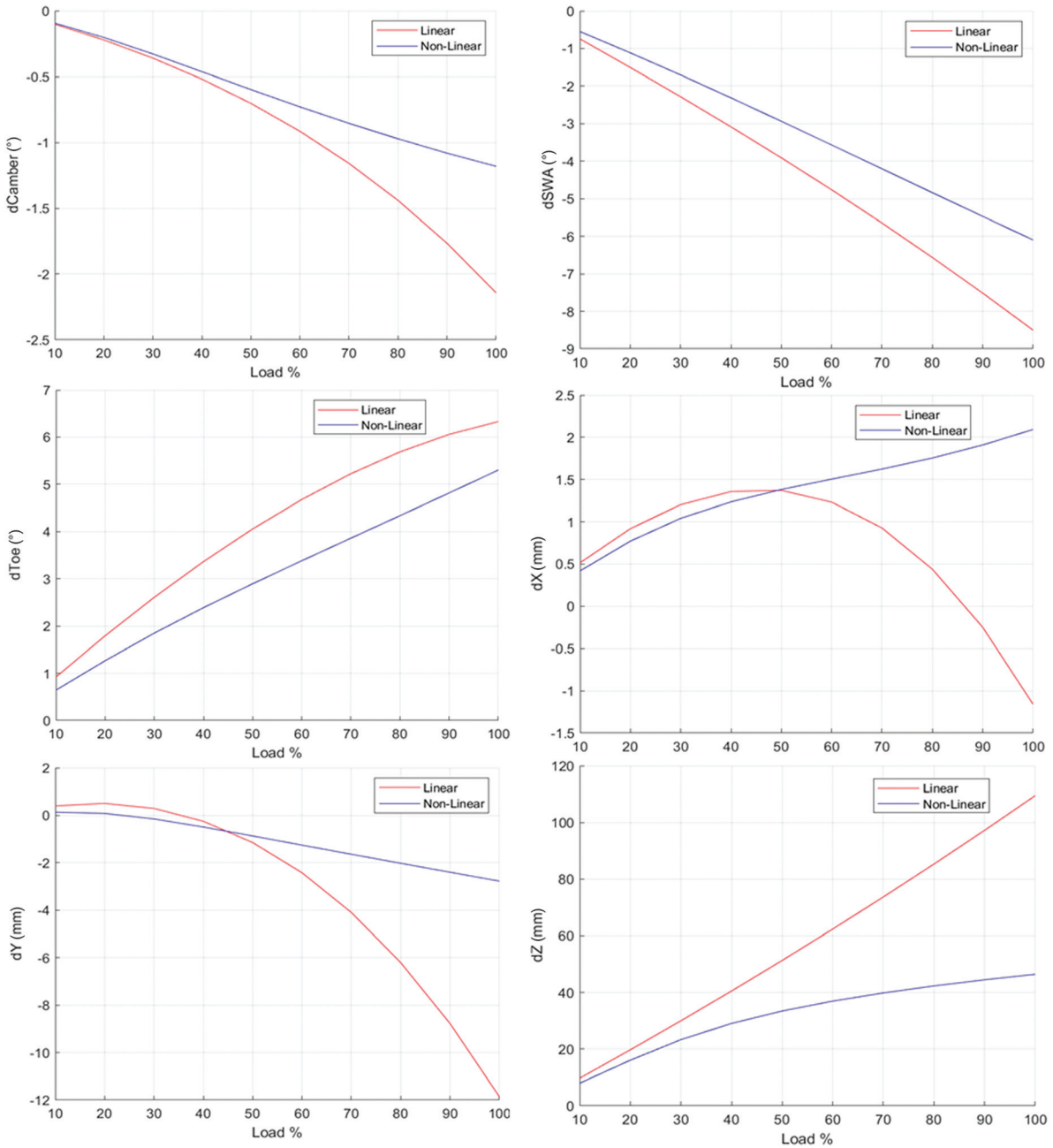

Fig. 14 Variation of wheel orientation (dCamber, dSWA, dToe) and position (*dX*, *dY*, *dZ*) at various % of the loadcase N8

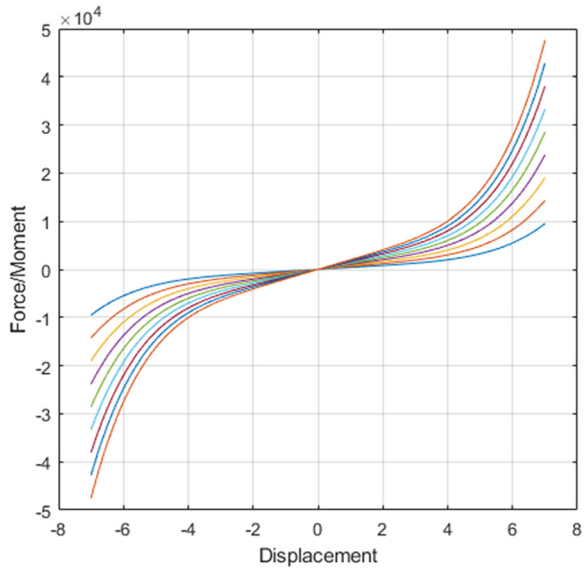

Fig. 15 Different chassis-side bushing force–displacement curves at different values of parameter K

of the same axle together, such as antiroll bars, which would in any case influence the compliance of the suspension during cornering. It is not possible to model suspensions with linkage and rockers, such as pushrods and pullrods, even though they are rather rare architectures in passenger cars.

Disclosure Statement

No potential conflict of interest was reported by the author(s).

Author Contribution Statement

Conceptualization, P.M., M.G.; methodology, P.M.; software, P. M.; data curation, P.M. and G.S.; writing—original draft preparation, P.M., M.G.; writing—review and editing, P.M., M.G., D.C. and G.S.; visualization, P.M., G.S. and D.C.; supervision, M.G. and D.C. All authors have read and agreed to the published version of the paper.

Data Availability Statement

The datasets generated and supporting the findings of this article are obtainable from the corresponding author upon reasonable request.

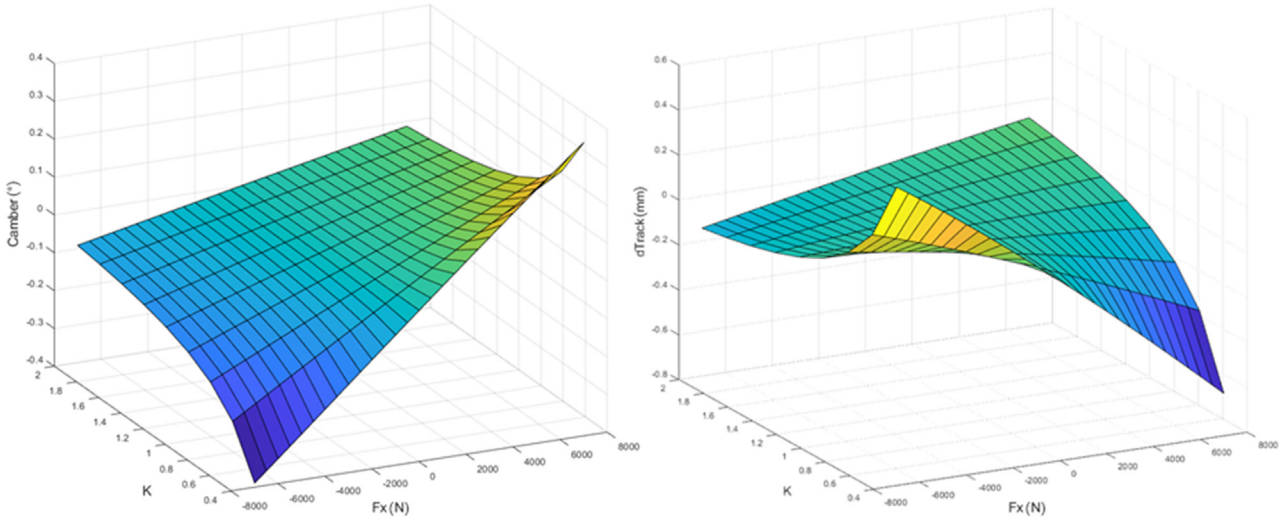

Fig. 16 Variation of camber (left side) and track (right side) as a function of *Fx* and the *K* parameter multiplying the chassis-side bushing force–displacement curve

of this algorithm in a driver-in-the-loop simulation. In this way, the effects of suspension compliance on the driving feeling can also be subjectively assessed via a driving simulator.

Looking at the comparison with the multibody software, the model seems to compute the solution correctly with low errors. The correlation coefficients appear to be essentially unitary. Qualitatively, by graphing the deformed configuration for different loads these are always practically overlapping, as can be seen in Figs. 9 and 10. The algorithm is intended to be a substitute for a multibody solver, but only in an initial design phase. In fact, this method is based on the search for the equilibrium position, it is therefore a quasi-static solver where dynamic effects such as inertia of the suspension elements or damping of the joints are not considered. Thus, a limitation of this algorithm is precisely the dynamic analyses, such as the evaluation of eigenfrequencies. The inclusion of these effects can be a future development, for example, by including forces dependent on the time derivatives of the element's deformations.

The method is designed to solve any type of independent wheel suspension. However, there are no elements connecting the wheels

References

[1] Von Der Ohe, M., 1983, "Front and Rear Suspension of the New Mercedes Model W201," SAE Paper No. 831045.
[2] Andersson, J. E., Bane, O., and Larsson, A., 1989, "Volvo 760 GLE Multi-Link Rear Axle Suspension," SAE Paper No. 890082.
[3] Kasahara, T., Morioka, N., Satou, M., Yagi, T., and Muraoka, K., 2000, "Development of a New Multi-Link Suspension," SAE Paper No. 01-0092.
[4] Koide, R., Kawabe, Y., Nakajima, K., and Kazuhiro, K., 2012, "Development of a New Multi-Link Rear Suspension," SAE Int. J. Passenger Cars - Mech. Syst., **5**(2), pp. 974–980.
[5] Jung, D., Lee, J. K., Lee, B. K., and Kim, S. P., 2013, "The Development of FR-Based 4WD Multi-Link Suspension," SAE Paper No. 01-1235.
[6] Zandbergen, P., and Girelli Consolaro, A., 2013, *Ford Motor Company's New Rear Suspension Architecture for the Global CD Platform*, (Proceedings of the FISITA 2012 World Automotive Congress, Lecture Notes in Electrical Engineering, Vol. 10), Springer, Berlin, Heidelberg, pp. 9–20.
[7] Gerrard, M. B., 1999, "Roll Centres and Jacking Forces in Independent suspensions - A First Principles Explanation and a Designer's Toolkit," SAE Paper No. 01-0046.
[8] Gerrard, M. B., 2002, "Kinematic Suspension linkages - A Model for Their Behaviour and a Procedure for Their Design," SAE Paper No. 01-0281.
[9] Balike, K. P., Rakheja, S., and Stiharu, I., 2009, "Kinematic Analysis and Parameter Sensitivity to Hard Points of Five-Link Rear Suspension Mechanism of Passenger Car," ASME Paper No.DETC2008-49243.

[10] Simionescu, P. A., and Beale, D., 2002, "Synthesis and Analysis of the Five-Link Rear Suspension System Used in Automobiles," Mech. Mach Theory, **37**(9), pp. 815–832.
[11] Simionescu, P. A., 2016, "A Unified Approach to the Kinematic Synthesis of Five-Link, Four-Link, and Double-Wishbone Suspension Mechanisms With Rack-and-Pinion Steering Control," Proc. Inst. Mech. Eng., Part D, **231**(10), pp. 1374–1387.
[12] Marchesin, F. P., Barbosa, R. S., Gadola, M., Chindamo, D., 2018, "High Downforce Race Car Vertical Dynamics: Aerodynamic Index," Veh. Syst. Dyn., **56**(8), pp. 1269–1288.
[13] Marchesin, F. P., Barbosa, R. S., Alves, M. A. L., Gadola, M., Chindamo, D., and Benini, C., 2016, "Upright Mounted Pushrod: The Effects on Racecar Handling Dynamics," Proceedings of the 24th Symposium of the International Association for Vehicle System Dynamics on The Dynamics of Vehicles on Roads and Tracks, IAVSD, Graz, Austria, Aug. 17–21, pp. 543–552.
[14] Marchesin, F., Barbosa, R. S., Gadola, M., and Chindamo, D., 2019, "A Road-Holding Index Based on Ride Dynamics for High-Downforce Racing Cars," IOP Conf. Ser. Mater. Sci. Eng., **538**(1), p. 012069.
[15] Gadola, M., Chindamo, D., Legnani, G., and Comini, M., 2019, "Teaching Automotive Suspension Design to Engineering Students: Bridging the Gap Between CAD and CAE Tools Through an Integrated Approach," Int. J. Mech. Eng. Educ., **47**(1), pp. 23–43.
[16] Bonera, E., Gadola, M., Chindamo, D., Morbioli, S., and Magri, P., "Integrated Design Tools for Model-Based Development of Innovative Vehicle Chassis and Powertrain Systems," Lecture Notes Mech. Eng., pp. 118–128.
[17] Knapczyk, J., and Dzierżek, S., 1995, "Displacement and Force Analysis of Five-Rod Suspension With Flexible Joints," ASME J. Mech. Des., **117**(4), pp. 532–538.
[18] Knapczyk, J., Dzierzek, S., 2007, "Elastokinematic Analysis of Five-Rod Suspension With Flexible Joints, Including Effects of Shock Absorber," Int. J. Veh. Mech. Mobility, **29**(S1), pp. 270–279.
[19] Knapczyk, J., and Maniowski, M., 2006, "Elastokinematic Modeling and Study of Five-Rod Suspension With Subframe," Mech. Mach Theory, **41**(9), pp. 1031–1047.
[20] Knapczyk, J., and Maniowski, M., 2010, "Optimization Of 5-Rod Car Suspension For Elastokinematic and Dynamic Characteristics," Archive Mech. Eng., **57**(2), pp. 133–147.
[21] Yang, X., 2011, "Effects of Bushings Characteristics on Suspension Ball Joint Travels," Veh. Syst. Dyn. **49**(1–2), pp. 181–197.
[22] Zhao, P., Yao, G. F., Wang, M., Wang, X., and Li, J., 2012, "A New Method to Calculate the Equivalent Stiffness of the Suspension System of a Vehicle," Struct. Eng. Mech., **44**(3), pp. 363–378.
[23] Yao, G. F., Hou, J., and Zhao, P., 2017, "A New Methodology to Calculate the Equivalent Stiffness Matrix of the Suspension Structure With Flexible Linkages," Adv. Mech. Eng., **9**(7), p. 168781401770054.
[24] Gerrard, M. B., 2005, "The Equivalent Elastic Mechanism: A Tool for the Analysis and the Design of Compliant Suspension Linkages," SAE Paper No. 1719.
[25] Kang, J. S., Yun, J. R., Lee, J. M., and Tak, T. O., 1997, "Elastokinematic Analysis and Optimization of Suspension Compliance Characteristics," SAE Paper No. 970104.
[26] Kang, J. S., 2005, "Elastokinematic Analysis of A Suspension System With Linear Recursive Formula," Int. J. Automot. Technol., **6**(4), pp. 375–381.
[27] Morales, E. D., 2016, "Sensitivity Study of Front Suspension Parameters in Elastokinematics and Handling Behavior of a Vehicle," SAE Paper No. 0812.
[28] Meissonnier, J., Fauroux, J. C., Gogu, G., Montezin, C., 2006, "Geometric Identification of an Elastokinematic Model in a Car Suspension," Proc. Inst. Mech. Eng., Part D, **220**(9), pp. 1209–1220.
[29] Rocca, E., Russo, R., 2002, "A Feasibility Study on Elastokinematic Parameter Identification for a Multilink Suspension," Proc. Inst. Mech. Eng., Part D **216**(2), pp. 153–160.
[30] Tang, L., Bin Shangguan, W., Dai, L., 2012, "A Calculation Method of Joint Forces for a Suspension Considering Nonlinear Elasticity of Bushings," Proc. Inst. Mech. Eng., Part K, **226**(4), pp. 281–297.
[31] Burgess, M. J., Fleming, N. P., Wootton, M., and Williams, S. J., 2004, "A Tool for Rapid Vehicle Suspension Design," SAE Paper No. 3543.